https://doi.org/10.5194/acp-2022-9
Preprint. Discussion started: 4 April 2022

Atmospheric Chemistry and Physics Discussions

Rapid reappearance of air pollution after cold air outbreaks in North China

Qian Liu[1], Guixing Chen[1], Lifang Sheng[2], Toshiki Iwasaki[3]

[1]School of Atmospheric Sciences, Sun Yat-sen University, and Southern Marine Science and Engineering Guangdong Laboratory (Zhuhai), Zhuhai, 519082, China
[2]Department of Marine Meteorology, College of Oceanic and Atmospheric Sciences, Ocean University of China, Qingdao, 266100, China
[3]Department of Geophysics, Graduate School of Science, Tohoku University, Sendai, 980-8577, Japan

Correspondence to: Dr. Guixing Chen (chenguixing@mail.sysu.edu.cn)

Abstract. The cold air outbreak (CAO) is the most important way to reduce air pollution during the winter over North China. However, a rapid reappearance of air pollution is usually observed during its decay phase. Is there any relationship between the reappearance of air pollution and the properties of CAO? To address this issue, we investigated the possible connection between air pollution reappearance and CAO by quantifying the properties of the residual cold airmass after CAO. Based on the analyses in recent winters (2014–2019), we found that the rapid reappearance of air pollution in the CAO decay phase has an occurrence frequency of 74%, and the air quality in more than 50% of CAOs worsens than that before CAO. The reappearance of air pollution tends to occur in the residual cold airmass with weak horizontal flux during the first two days after CAO. By categorizing the CAOs into groups of rapid and slow air pollution reappearance, we found that the residual cold airmass with moderate depth of 150–180 hPa, large negative heat content and small slopes of isentropes is favorable for the rapid reappearance of air pollution. Among these factors, the cold airmass depth is highly consistent with the mixing layer height, below which contains most air pollutants; the negative heat content and slope of isentropes in cold airmass jointly determine the intensity of low-level vertical stability. The rapid reappearance of air pollution is also attributed to the maintenance of residual cold airmass and the above conditions, which is mainly regulated by the dynamic transport process rather than diabatic cooling or heating. Furthermore, analysis of the large-scale circulation of CAOs in their initial stage shows that the anticyclonic (cyclonic) pattern in northern Siberia (northeastern Asia) can be recognized as a precursor for the rapid (slow) reappearance of air pollution after the CAO.

https://doi.org/10.5194/acp-2022-9
Preprint. Discussion started: 4 April 2022


Atmospheric Chemistry and Physics Discussions

1 Introduction

Air pollution is one of the main meteorological disasters in China during the boreal winter, threatening public health, the environment and economic activities (Guan et al., 2016; Xu et al., 2013; Tie et al., 2016). North China, experiences the most pollution, resulting in attention from researchers. Statistics show that air pollution or haze events in North China have an occurrence frequency of approximately 20–40 days during winters since 2010 (Ding and Liu, 2014; Chen and Wang, 2015; Yang et al., 2016; Dang and Liao, 2019; Zhang et al., 2020). In some cities, such as Beijing, the occurrence frequency approached 60 days (Li et al., 2021). Moreover, severe air pollution has also occurred frequently over North China in recent years, during which the air quality index usually exceeds the upper limit. In some widely reported air pollution events during January 2013, December 2015 and December 2016, the regional daily mean $PM_{2.5}$ concentration exceeds 500 μg m^{-3} (Zhang et al., 2014; Sun et al., 2016; Yin and Wang, 2017). Faced with the demands of improving air quality, progress in understanding the variations in air pollution is of great importance.

The formation of air pollution in North China can be attributed to heavy emissions, topography and unfavorable meteorological conditions (Zhang et al., 2013; Cao et al., 2015; Yang et al., 2016; Dang and Liao, 2019; An et al., 2019). As emissions and topography do not vary much from day to day, meteorological conditions play an important role in impacting synoptic time-scale variations in air pollution (Kang et al., 2019; Ma et al., 2021; Zhang et al., 2021). Previous studies showed that weak surface winds, high relative humidity, enhanced temperature inversion, low atmospheric boundary layer height, and less precipitation facilitate the accumulation and maintenance of air pollutants (Ding and Liu, 2014; Wang and Chen, 2016; Li et al., 2017). These unfavorable meteorological conditions usually occur in stagnant weather controlled by high-pressure systems or anomalous anticyclonic patterns (Yang et al., 2018; Zhong et al., 2019; An et al., 2020).

Cold air outbreaks (CAOs) are generally considered to be conducive to the removal of air pollution in North China (Qu et al., 2015; Li et al., 2016; Liu et al., 2017; Hu et al., 2018; Zhang et al., 2021). However, our recent study shows that air pollutant concentrations sometimes experienced a rapid increase after CAO, forming a new round of air pollution with even higher pollutant concentrations than the period before CAO (Liu et al., 2019). During the reappearance of air pollution, the regional mean pollutant concentrations increased as much as 2.8 times. Some studies also provided clues for the reappearance of air pollution after CAO. Under high emissions conditions, the removal of air pollution caused by strong surface winds is usually maintained for only approximately 1 day and then returns to the polluted state rapidly (Liu et al., 2016). Wang et al. (2014) showed that during persistent heavy air pollution in January 2013, cold air activity could only temporarily reduce the air pollutant concentration. The reappearance of air pollution is usually characterized by explosive growth, with air pollutant concentrations increasing from a few to tens and even hundreds of micrograms per cubic meter within 1 day (Sun et al., 2016). These results suggest that a considerable portion of air pollution in North China can be linked to the decay of the CAO. To explore the mechanisms modulating rapid increases in air pollutants, further analysis showing the detailed features and structures of CAOs, especially during their decay stages, is required. Additionally, since CAOs are easy to identify and predict in their initial stages, they also have potential as precursory signals for the burst of severe air pollution.

https://doi.org/10.5194/acp-2022-9
Preprint. Discussion started: 4 April 2022


Atmospheric Chemistry and Physics Discussions

In this study, a quantitative measurement of cold airmass (Iwasaki et al., 2014) is adopted to identify CAO and its dynamic/thermodynamic characteristics. Based on the analyses of CAOs and accompanying variations in air pollution during recent winters, our study will verify the generic existence of air pollution reappearance after CAO. Then, we will clarify the CAO with what characteristics, such as depth, horizontal flux, coldness and large-scale circulation pattern of cold airmass, may result in the rapid reappearance of air pollution. The rest of this study is organized as follow. The data and methods used in this study are described in Section 2. Statistical features of air pollution reappearance, as well as its association with CAO evolution, are examined in Section 3. The key features of CAO affecting the air pollution reappearance and the involved physical mechanisms are discussed in Section 4. Section 5 further investigates the large-scale circulation pattern of the CAO. A short summary is presented in Section 6.

2 Data and methods

2.1 Data

The variation in air pollutant concentration in this study is described using the air quality index (AQI) from the Ministry of Ecology and Environment of the People Republic of China. The AQI quantifies overall air quality based on the primary air pollutant in the monitored area, with observations made 24 times per day. Data from 475 stations (in 98 cities) across North China (30°–40°N, 114°–122°E) covering the winters (November to March) from 2014/2015 to 2018/2019 were used. The sounding data, including wind and air temperature, are obtained from the University of Wyoming. Four sounding stations were selected in North China: Beijing (39.8°N, 116.5°E), Zhangqiu (36.7°N, 117.6°E), Nanjing (31.9°N, 118.9°E) and Baoshan (31.4°N, 121.5°E). Observation times were 00 and 12 UTC (08 and 20 LT).

To identify the CAO events, we used Japanese 55-year reanalysis (JRA-55) data. The JRA-55 has a horizontal resolution of 1.25° with 37 vertical pressure levels and a time interval of 6 hours. Previous studies have shown that JRA-55 has good performance in identifying and describing CAOs over East Asia (Yamaguchi et al., 2019; Liu et al., 2020; Liu et al., 2021).

2.2 Isentropic analysis of cold air outbreak

The identification and quantification of cold airmass and its outbreaks are performed by an isentropic analysis method. The cold airmass is defined as a layer of airmass below the threshold isentropic surface of $\theta_T = 280$ K, which includes most of the equatorward cold airmass flow (Iwasaki et al., 2014). Thus, the depth of the cold airmass (DP) can be described as the pressure difference between the ground surface (p_s) and the θ_T surface ($p(\theta_T)$),

$$DP = p_s - p(\theta_T). \quad (1)$$

The horizontal flux of the cold airmass (F) is given by the vertical integral of the horizontal wind (v) and the pressure (p),

$$F = \int_{p(\theta_T)}^{p_s} v\, dp. \quad (2)$$

https://doi.org/10.5194/acp-2022-9
Preprint. Discussion started: 4 April 2022


Atmospheric Chemistry and Physics Discussions

The negative heat content (NHC), reflecting the coldness of the cold airmass, is defined as a vertical integral of the potential temperature difference ($\theta_T - \theta$) and pressure (p),

$$NHC = \int_{p(\theta_T)}^{p_s} (\theta_T - \theta)\, dp. \quad (3)$$

Based on the above method, the CAO can be identified by the regional mean cold airmass depth. Previous studies showed that the cold airmass depth usually experiences a sharp increase and reaches a relatively high value during the outbreak (Shoji et al., 2014; Liu et al., 2019; Liu et al., 2021). Thus, the CAO in this study is identified when the regional mean cold airmass depth exceeds 169.7 hPa, which is the standard deviation of cold airmass depth on all winter days. According to the above criteria, 39 CAOs are identified over the 5 winters.

The CAO is further divided into 3 periods. Figure 1 shows the temporal evolution of the cold airmass depth in North China during a typical CAO in March 2016. The period during the CAO is defined as the days with cold airmass depths higher than one standard deviation (169.7 hPa). The onset of a CAO event, which is the first day of the period during CAO, is described as the day 0. The period before CAO is defined as the two days before onset day and the onset day (days −2 to 0). The period after CAO, which is also called the decay phase, is defined as the three days following the period during the CAO. It should be noted that the cold airmass in the period after CAO is called the residual cold airmass in this study.

2.3 Measurement of air pollution reappearance and mixing layer height

The description of air pollution reappearance is based on the AQI in different periods of the CAO, as shown in Figure 1. In the period before CAO, the AQI decreases from a polluted state to a relatively clean state. The AQI usually reaches its minimum in the period during CAO. Then, the AQI increases and results in a new round of air pollution in the period after CAO. Thus, we use the maximum AQI in the period before CAO (AQI_b) and the maximum AQI in the period after CAO (AQI_a) to represent the air pollution before CAO and the reappeared air pollution, respectively. The minimum AQI in the period during CAO (AQI_d) is used to represent the clean state between the air pollutions before and after the CAO.

Based on the above analysis, the increase of AQI (IA) is defined as follows to describe the deterioration rate of air pollution in its reappearance:

$$IA = AQI\_a - AQI\_d. \quad (4)$$

A rapid reappearance of air pollution is supposed to have an IA larger than 35.5, which is the standard deviation of the AQI daily variation during the 5 winters. A reappearance index of air pollution (RI) is also defined to describe the relative intensity of reappeared air pollution compared to the air pollution before CAO,

$$RI = AQI\_a/AQI\_b, \quad (5)$$

where RI larger (smaller) than 1 denotes that the AQI after CAO is worse (better) than that before CAO.

The mixing layer height is determined from the analysis of the profile of the bulk Richardson number (R_B) using sounding data. The calculation method for R_B is derived from Tang et al. (2016) as follows:

https://doi.org/10.5194/acp-2022-9
Preprint. Discussion started: 4 April 2022


Atmospheric Chemistry and Physics Discussions

$$R_B = \frac{g\,\Delta\theta\,\Delta Z}{\theta\,((\Delta u)^2+(\Delta v)^2)}, \quad (6)$$

where g, θ, Z, u and v indicate the gravity acceleration, potential temperature, height, zonal wind and meridional wind, respectively. According to the profiles of R_B and θ, the observations can be separated into a convective state and a stable state. In this study, we found that all the sounding observations are in the stable state with no obvious low-level jet. Therefore, the mixing layer height (MLH) is defined as the altitude at which R_B is greater than 1.

3 Characteristics of air pollution reappearance after CAO

3.1 Statistics of AQI after CAO

To ensure the existence of the rapid reappearance of air pollution after CAO, the relationship of daily changes in AQI and cold airmass depth is divided into four quadrants in Figure 2. In winter, 64.2% of the decrease in the AQI occurs when the cold airmass depth increases, which corresponds to the period before and during the CAO. On the other hand, most of the AQI increase (71.0%) was accompanied by a cold airmass decrease, which usually occurred in the period after the CAO. Based on these results, the AQI variation changes from decreasing to increasing throughout the CAO, suggesting the existence of air pollution reappearance after the CAO. We also noticed that most of the heavy air pollution was in the quadrant of cold airmass depth decrease, suggesting that the retreat and dissipation of cold airmass may be an important meteorological factor for the formation of heavy air pollution.

Based on the 39 CAOs selected in this study, the statistical characteristics of the air pollution reappearance after CAO can be demonstrated. Figure 3a compares the AQI daily change rate in the period after CAO to that on all winter days. During the period after CAO, the increase in the AQI has an occurrence frequency of more than 80%, which is much higher than that on all winter days (56%). In particular, the relatively high increase rate (> 20 day^{-1}) in the period after CAO has a frequency of approximately twice as high as that on all winter days. Such a frequent rapid increase in the AQI after CAO could induce the reappearance of air pollution and even may result in a worse AQI compared to the AQI before CAO. Using the Eq. (5), Figure 3b shows the reappearance rate of air pollution (RI) after CAO, whose value greater (smaller) than 1 denotes that the AQI after CAO is worse (better) than the AQI before CAO. More than 50% of the CAOs are found to show a worse AQI after reappearance. In some extreme events, the AQI after CAO could be twice as high as the AQI before CAO. These facts show that even if the CAO brings several days of clean air, it may lead to a deterioration of the AQI to the polluted or an even worse state.

Considering the different characteristics of AQI variations after the CAO, the CAOs can be categorized into a “slow reappearance” group and a “rapid reappearance” group according to the variable defined by Eq. (4) (Figure 3c). Among the 39 CAOs, 10 (25.6%) show a slow reappearance of air pollution after CAO (CAO_slow), with an increase in the AQI of less than 1 standard deviation of the AQI daily variation ($IA \leq 35.5$). Note that not all CAOs are accompanied by a rapid air pollution reappearance. The remaining 29 CAOs (74.4%) featured a rapid reappearance of air pollution (CAO_rapid). Figure

https://doi.org/10.5194/acp-2022-9
Preprint. Discussion started: 4 April 2022


Atmospheric Chemistry and Physics Discussions

3c also shows that most CAO_slow events have a better AQI than that before CAO, while nearly two-thirds of CAO_rapid events face a worse AQI. The above differences in AQI changes after CAO suggest that the air pollution reappears rapidly or slowly may be modulated by the detailed characteristics of CAO.

3.2 Relationship between the reappearance of air pollution and CAO

In terms of spatial averages over North China, Figure 4 shows large differences in the cold airmass depth and AQI between CAO_rapid and CAO_slow events. For CAO_rapid events (Figure 4a), the cold airmass depth increases from day −2 and reaches its maximum on day 0. Then, the cold airmass depth gradually decreases to approximately 100 hPa in the following 3 days. During the whole life cycle of the CAO_rapid event, the AQI shows a reversed variation to cold airmass depth. From day −2 to day 0, the AQI fell to a moderate level below 70. However, shortly after, the AQI increased rapidly to nearly 130 on day +2, which was worse than the AQI before the CAO. For CAO_slow events (Figure 4b), the cold airmass depth also increases from day −2 to day 0 and reaches a value similar to that in CAO_rapid events. After day 0, the cold airmass depth drops to the minimum on day +2 at a much faster rate than that in CAO_rapid events and rises again from day +3. During the CAO_slow events, the AQI still varies conversely to the cold airmass depth. However, the decrease in the AQI starts on day 0, which is later than that in CAO_rapid events, and the variation in the AQI also has a relatively small amplitude. Such differences in the removal of air pollution may be associated with the thermal/dynamical features of CAO (Liu et al., 2019). The contrasts of the CAO_rapid and CAO_slow events suggest that there may be two favorable conditions for the rapid air pollution reappearance: one is the relatively slow decrease of cold airmass depth, the other is the longer time period before the next CAO.

We further investigate the spatial-temporal collocation of the AQI and cold airmass distributions during and after the CAO. For CAO_rapid events, a thick layer of cold airmass accompanying the strong southeastward flux is observed in North China on day 0 (Figures 5a–5b). At this stage, the AQI decreased markedly, especially in the eastern part of North China. From day +1 to day +3, the southeastward flux of cold airmass weakens, and a quasi-stationary residual cold airmass occupies North China (Figures 5c–5h). During this period, the AQI increased rapidly and even exceeded 150 (middle level air pollution) at a number of stations. The worst AQI usually occurs in the region with a cold airmass depth of 50–150 hPa. For CAO_slow events on day 0, the cold airmass depth has a distribution similar to that in CAO_rapid events (Figures 6a–6b). However, the cold airmass fluxes in CAO_slow events contain a larger eastward component than those in CAO_rapid events. Such an enhanced eastward flux leads to the quick eastward retreat of residual cold airmass on days +1 and +2 (Figures 6c–6f). During this period, an increase in the AQI is also observed in the area covered by the residual cold airmass. On day +3, the cold airmass enhances again in the northern part of North China and thus ends the reappearance of air pollution (Figures 6g–6h). According to the above results, we found that the reappearance of air pollution tends to occur in the residual cold airmass with nearly no horizontal flux during the decay period of the CAO.

https://doi.org/10.5194/acp-2022-9
Preprint. Discussion started: 4 April 2022

4 Factors affecting the rapid reappearance of air pollution

To determine the dominant feature of CAO controlling the reappearance of air pollution, Table 1 compares the dynamic and thermal-dynamic properties of cold airmass in CAO_rapid and CAO_slow events. The cold airmass properties are averaged in the period from day +1 to +2, which corresponds to the rapid increase period of the AQI in Figure 4. The results reveal that the magnitude of cold airmass flux shows a small difference between the two types of CAO. However, large differences exist in the depth and NHC of cold airmass, which may be the key factors affecting the air pollution reappearance. The cold airmass in CAO_rapid events (140.9 hPa and 718.8 K hPa) is thicker and colder than that in CAO_slow events (116.0 hPa and 431.9 K hPa). To explore how the depth and NHC of cold airmass modulate the air pollution reappearance, a CAO_rapid event (14–17 December 2016) and a CAO_slow event (11–14 February 2018) are selected for further analysis.

Table 1: Averaged AQI change rate and cold airmass properties during the period from day +1 to +2.

	Change rate of AQI (day^{-1})	Cold airmass depth (hPa)	Magnitude of cold airmass flux (hPa m s^{-1})	Negative heat content (K hPa)
CAO_rapid	23.4	140.9	872.9	718.8
CAO_slow	14.4	116.0	823.3	431.9

4.1 Cold airmass depth

Figures 7 and 8 examine the profile of potential temperatures below 3 km at the four stations (see Section 2.1) under the effect of the CAO. During the CAO_rapid event on day 0, the lapse rate of potential temperature is small from the near ground level to the height of approximately 1.5 km (Figure 7a). Above the height of 1.5 km, the lapse rate suddenly increases, forming an air layer with a large vertical gradient of potential temperatures. Such a large vertical gradient of potential temperature denotes a strong stable stratification, weakening the vertical mixing of air pollutants to the upper level. In the case of high emissions in North China (Zhang et al., 2012; Gao et al., 2016), atmospheric conditions such as this are favorable for the accumulation of air pollutants in the near surface atmosphere. On the other hand, the large gradient layer can be recognized as the upper boundary of the cold airmass since the cold airmass features strong thermal contrast to its surroundings. This upper boundary of cold airmass acts as a lid confining the air pollutant in the residual cold airmass. Previous studies also show that air pollutants usually increase and are trapped in the residual cold airmass during the period after CAO (Kang et al., 2019; Liu et al. 2019). From day 0 to +1, the height of the large gradient layer is maintained at approximately 1.5 km, and then it slowly drops to 0.5 km in the following 2 days. Such a temporal evolution is highly consistent with the evolution of cold airmass depth (Figures 7a and 7b). In the same period, the AQI increases nearly 2 times from 50 to 150.

https://doi.org/10.5194/acp-2022-9
Preprint. Discussion started: 4 April 2022


Atmospheric Chemistry and Physics Discussions

The low-level atmosphere with a small lapse rate of potential temperature in Figure 7a may represent the mixing layer, featuring convection, vertical mixing and dry-adiabatic lapse rates. The mixing layer could greatly impact the accumulation and dissipation of air pollutants (Holzworth, 1967; Tang et al., 2016). Many studies have reported that the MLH is a good indicator of air quality (Su et al., 2018; Gui et al., 2019). However, the calculation of MLH is somewhat complex (Eq. (6)), and the MLH calculated by most mainstream reanalysis datasets has obvious bias compared to sounding data (Guo et al., 2021). Figure 7b shows the MLH at the four stations at 12 UTC. The MLH and cold airmass depth have good agreement in both values and temporal variations. This is because the vertical structures of temperature and wind in the low-level atmosphere are mainly forced by the cold airmass during CAO. Thus, the residual cold airmass happens to be the mixing layer and modulates the evolution of the AQI. In addition, the calculation of cold airmass depth using reanalysis data is much easier than the calculation of MLH using sounding or other observation data, suggesting that the cold airmass depth may be a good substitute for MLH in periods during and after the CAO.

In the CAO_slow event on day 0, the potential temperature has a profile similar to that in the CAO_rapid event (Figure 8a). The large gradient layer is located at approximately 2.5 km, which corresponds to the cold airmass depth and MLH (Figure 8b). Such features in cold airmass and atmospheric stratification continue to 00 UTC on day +1. During this period, the AQI shows no increase due to the high MLH. From day +1 to +2, the cold airmass depth decreases rapidly and almost disappears in the southern part of North China, leading to the disappearance of the large gradient layer in low troposphere. It should be noted that the mixing layer at this time is not forced by residual cold airmass since it is absence. As the MLH decreases to 1.5 km, the AQI experiences a relatively slow increase. On day +3, the cold airmass depth increases again, causing an increase in the MLH and a decrease in the AQI.

Based on the analyses of a CAO_rapid event and a CAO_slow event, we conclude that the intrusion of cold airmass forces the lower troposphere into a stable stratification that is favorable for the increase in the AQI. Thus, the depth and persistence of the residual cold airmass were thought to be two factors that influence the deterioration rate of air pollution. It is clear that a longer persistence of residual cold airmass is favorable for the rapid reappearance of air pollution, while the relation between cold airmass depth and the AQI increase rate is quite complex. Regarding the rapid reappearance of air pollution, the cold airmass depth is not the lower the better. In CAO_rapid events, for example (Figure 5), the increase in the AQI is less obvious in the region to the south of North China (25°–30°N) with a cold airmass depth thinner than 100 hPa. Moreover, the AQI increase rate will not vary monotonically with cold airmass depth. The AQIs in Yangtze River Delta (30°–32°N, 118°–122°E) and Bohai Rim (37°–40°N, 117°–122°E) have similar increase rates, although the Bohai Rim has a cold airmass depth much thicker than that of the Yangtze River Delta. Similar results can also be found in CAO_slow events (Figure 6). According to these analyses, Figure 9 presents the relation between cold airmass depth and the AQI change rate. With increasing cold airmass depth, the change rate of the AQI first increases and then slightly decreases. A cold airmass depth that is too thick dilutes the surface air pollutant concentration, but a cold airmass depth that is too thin damages the persistence of the cold airmass. The cold airmass depth in a moderate range of 150–180 hPa (approximately 1.5–1.8 km) is most favorable for the air

https://doi.org/10.5194/acp-2022-9
Preprint. Discussion started: 4 April 2022


Atmospheric Chemistry and Physics Discussions

240 pollution reappearance, with a mean increase rate of 32.1 day^{-1}. In some extreme cases exceeding the 90th percentile, the AQI increase rate can reach 80 day^{-1}.

4.2 NHC and vertical thermal structure

As another key factor revealed in Table 1, NHC also contributes to air pollution reappearance. According to the definition in Section 2.2 (Eq. (3)), NHC is proportional to the production of cold airmass depth (DP) and vertical averaged potential
245 temperature difference ($\Delta\theta = \overline{(\theta_T - \theta)}$). If the potential temperature increases linearly with height, $\Delta\theta$ can be further simplified as $(\theta_T - \theta_s)$, where θ_s is the surface potential temperature. Here, diving the NHC by $(DP)^2$ lead us to the following:

$$\frac{NHC}{(DP)^2} \propto \frac{\Delta\theta}{\Delta p}\Big|_{Cold\ airmass}, \quad (7)$$

where Δp is equal to DP when referring to the cold airmass, and $\frac{\Delta\theta}{\Delta p}$ indicates the averaged vertical stability in the cold airmass. Thus, at a given cold airmass depth (DP), a larger NHC will likely result in a more stable stratification, which is favorable for
250 air pollution reappearance. This explains why the NHC is much larger during the decay period in CAO_rapid events than in CAO_slow events (Table 1). On the other hand, the persistence of cold airmass will also benefit from the large NHC, which helps to dampen the reduction effect of diabatic heating.

In addition to NHC, the two selected CAO events show that the vertical thermal structure of cold airmass also influences the stability of low-level troposphere (Figure 10). On the onset day of the CAO_rapid event (Figure 10a), the upper boundary of
255 cold airmass is relatively flat, rising from 900 hPa at 30°N to 770 hPa at 40°N. Inside the cold airmass, the isentropes represented by the potential temperature anomaly are essentially parallel to the upper boundary of cold airmass. Such flat distributions indicate that the vertical gradient is the dominant component of the potential temperature gradient. As a result, a strong stable layer forms at the upper part of cold airmass spanning 900–700 hPa. Note that this large vertical gradient layer can also be seen in Figure 7a. After the outbreak on day +1 (Figure 10b), the upper boundary of cold airmass remained almost
260 unchanged, and the negative anomaly of potential temperature weakened slightly. The stable layer still exists at the upper part of cold airmass, although its intensity is weaker than that on day 0. For the CAO_slow event on day 0 (Figure 10c), the upper boundary of cold airmass steeply increases from 900 hPa at 30°N to higher than 600 hPa at 40°N. The slope of cold airmass in the CAO_slow event is more than twice that in the CAO_rapid event. The isentropes in the cold airmass are almost perpendicular below 850 hPa. In this scenario, the vertical gradient of potential temperature is small in the CAO_slow event,
265 even if it has a thicker and colder cold airmass than that in the CAO_rapid event. Accordingly, a stable layer with smaller intensity but higher altitude (800–600 hPa) is observed over the central and southern parts of cold airmass. On day +1 (Figure 10d), the cold airmass depth decreases markedly; however, the slope of isentropes remains large. As a result, the relatively weak stable layer lowers to approximately 850 hPa.

The differences in vertical atmospheric stability may lead to different increase rates of AQI during air pollution reappearance.
270 Figure 11 compares the evolutions of vertical stability in North China during the two CAO events. From 00 UTC day 0 to 12

https://doi.org/10.5194/acp-2022-9
Preprint. Discussion started: 4 April 2022


Atmospheric Chemistry and Physics Discussions

UTC day +1, the CAO_rapid event has a larger stability than that in the CAO_slow event at both the upper boundary and the entire cold airmass. In particular, the stability of the entire cold airmass in the CAO_rapid event is twice as high as that in the CAO_slow event. During this period, the AQI in the CAO_rapid event increases drastically from 50 to 120 under strong stable stratification, while the AQI in the CAO_slow event remains in the range of 80–100 under weak stable stratification (Figures 7b and 8b). After 12 UTC day +1, the variation in the AQI becomes steady, while the atmospheric stability starts to increase (Figure 11). This may be attributed to the radiative feedback of the air pollutant (Petäjä et al., 2016; Ding et al., 2016). By comparing the two types of CAO events, we find that the NHC and vertical structure of cold airmass jointly affect the low-level vertical stability, which modulates the air pollution reappearance. A cold airmass with a small slope of isentropes and a large NHC is favorable for the rapid reappearance of air pollution.

4.3 Possible mechanisms governing key features of cold airmass

Since the properties of the residual cold airmass control the features of air pollution reappearance. It is necessary to investigate the possible mechanisms modifying cold airmass changes during the decay period of the CAO. According to Iwasaki et al. (2014), the total cold airmass conservation equation can be described as follows:

$$\frac{\partial DP}{\partial t} = -\nabla \cdot \int_{p(\theta_T)}^{p_s} v\, dp + G(\theta_T). \quad (8)$$

The change in cold airmass depth is caused by the horizontal convergence/divergence of the cold airmass flux ($-\nabla \cdot \int_{p(\theta_T)}^{p_s} v\, dp$) and the vertical flux crossing the θ_T surface ($G(\theta_T)$). The former represents the dynamic process, and the latter is related to diabatic cooling and heating.

Based on Eq. (8), Figure 12 compares the composited evolutions of cold airmass changes induced by dynamic and diabatic processes. During the CAO_rapid events (Figure 12a), the decrease in cold airmass is mainly attributed to the dynamic process, which shows a decreasing effect since 18 UTC day 0 and reaches a maximum of −83.7 hPa day^{-1} at 18 UTC day +1. The effect of the diabatic process on cold airmass exhibits obvious diurnal variation, cooling/increasing the cold airmass at night (12–24 UTC) and heating/decreasing the cold airmass during the daytime (00–12 UTC). On days 0 and +1, the diabatic heating is weak during the daytime, inducing a slight net increase in cold airmass caused by the diabatic process. From day +2, the heating effect intensifies and reduces the cold airmass jointly with the dynamic process. During the decaying period of cold airmass on days +1 and +2, the average effects of dynamic and diabatic processes on cold airmass are −56.9 and 7.7 hPa day^{-1}, respectively.

For CAO_slow events (Figure 12b), the dynamic process still dominates in the cold airmass decrease. The average tendencies of dynamic and diabatic processes on days +1 and +2 are −71.8 and 4.8 hPa day^{-1}, respectively. The two types of processes show similar variations but larger amplitudes compared to those in CAO_rapid events. For the effect of the diabatic process, a much stronger diurnal variation is observed. This may be related to the relatively small potential temperature lapse rate and NHC in CAO_slow events (Figure 11 and Table 1). Strong diabatic heating also shows a notable contribution to the cold airmass reduction during the daytime, although the daily average effect of the diabatic process is relatively small. For the

https://doi.org/10.5194/acp-2022-9
Preprint. Discussion started: 4 April 2022


Atmospheric Chemistry and Physics Discussions

decrease in cold airmass associated with the dynamic process, the decreasing rate in CAO_slow events could reach a maximum rate of −110.1 hPa day^{-1}, which is 31.5% higher than that in CAO_rapid events. This enhanced contribution of the dynamic process can be related to the strong easterlies in the cold airmass, which are illustrated in the bar charts of Figure 10. The strong eastward transport from North China to the marine area quickly reduced the cold airmass depth in the CAO_slow events.

5 Discussion: large-scale circulation pattern of the CAO associated with the rapid reappearance of air pollution

In this section, we further check the large-scale circulation pattern of the CAO to see if we can find precursors for rapid air pollution reappearance. Figure 13 shows the composited spatial evolutions of cold airmass depth and flux during the initial stages (days −4 to 0) of CAO_rapid and CAO_slow events. For CAO_rapid events (Figure 13a), an anticyclonic pattern of anomalous cold airmass flux appears in northern Siberia (60°–80°N, 70°–120°E) on day −4. To the south of this anomalous anticyclone near Lake Baikal, the cold airmass depth shows a positive anomaly. In the following two days, the anticyclone intensifies in strength and extends from the high latitudes to the middle latitudes covering most of Siberia. The strong southward flux of cold airmass on the eastern flank of the anticyclone induces an increase in cold airmass depth and guides the cold airmass to move southeastward. From day −1 to day 0, the anticyclonic pattern gradually disappears, while the strong southward flux on its eastern flank is strengthened and extends further south. Driven by this southward cold airmass flux, the cold airmass depth anomaly dominates North China.

The CAO_slow events have distinct features in circulation patterns different from CAO_rapid events (Figure 13b). On day −4, a cyclonic pattern of anomalous cold airmass flux is observed in northeastern Asia, which is also featured by the positive anomaly of cold airmass depth. Meanwhile, a southward flux of cold airmass with cyclonic curvature can be found to the northwest of Lake Baikal (55°–70°N, 80°–100°E). During days −3 and −2, the cyclonic pattern and corresponding cold airmass depth anomaly over northeastern Asia weakens and moves to the Northwest Pacific. The southward cold airmass flux near Lake Baikal intensifies rapidly and forms a new cyclonic pattern in northeastern Asia. Along with the strengthening of the new cyclonic pattern, a positive anomaly of cold airmass depth occurs and increases rapidly. In the following days, the newly formed cyclonic pattern and anomalous cold airmass depth continued to intensify and swept into North China.

The above results suggest that CAO_rapid and CAO_slow events are distinguished by the dominant pattern of large-scale anomalous cold airmass flux in the early period of the CAO (days −4 to −2). The CAO_rapid events feature an anticyclonic pattern in northern Siberia, while CAO_slow events are dominated by a cyclonic pattern in northeastern Asia (Figure 10). The circulation patterns of CAO_rapid and CAO_slow events are also reported as the two main types of CAOs in East Asia, which account for 27% and 26% of the total frequency, respectively (Liu et al., 2021). Such differences in large-scale circulation patterns have a close association with the evolution of cold airmass after CAO. For CAO_rapid events, the southward flux at the eastern flank of the anticyclone is favorable for the maintenance of cold airmass in North China (Figures 5, 12a and 13a). For CAO_slow events, however, the cold airmass flux at the southern flank of the cyclone contains a large eastward component,

https://doi.org/10.5194/acp-2022-9
Preprint. Discussion started: 4 April 2022


Atmospheric Chemistry and Physics Discussions

causing a fast departure of cold airmass from North China (Figures 6, 12b and 13b). Therefore, the anticyclonic and cyclonic patterns in high-latitude Eurasia can be used as precursors for the estimation of air pollution reappearance after the CAO.

6 Conclusions

The CAO is well known to have a strong removal effect on air pollution over North China. However, air pollution may experience a rapid reappearance after the CAO and even lead to worse pollution. Based on the AQI measurement and quantitative description of cold airmass during the last 5 winters, the detailed characteristics and possible causes of air pollution reappearance after 39 CAOs are analyzed. During the period after the CAO, the increase in the AQI in North China has a probability of more than 80%, and the AQI increase rate is much faster than that in other periods in winter. In more than half of CAOs, the AQI in reappeared air pollution is worse than the AQI before CAO. The CAOs are divided into a "rapid reappearance" group (74.4%) and a "slow reappearance" group (25.6%) by the increase rate in the AQI. CAO_rapid events tend to have a relatively slow decrease in cold airmass depth and a long interval time before the next CAO. Spatiotemporal evolution shows that the reappearance of air pollution usually occurs in the first two days after CAO. The region of worst AQI after the air pollution reappearance features a slowly decreasing residual cold airmass with nearly no horizontal flux.

The rapid reappearance of air pollution is mainly attributed to the stable stratification in the lower troposphere forced by the intrusion of cold airmass. A comparison of the two groups of CAOs shows that the depth, NHC and vertical structure of cold airmass are key features modulating the reappearance of air pollution. The cold airmass depth could well present the MLH and has good agreement with the MLH in both value and variation. A moderate depth (150–180 hPa) of cold airmass is most favorable for air pollution reappearance since it is thin enough to restrict the spread of air pollutants and thick enough to maintain its own existence. The NHC is proportional to the vertical stability and persistence of the cold airmass. For a fixed cold airmass depth, a larger NHC will lead to a more rapid reappearance of air pollution. The vertical structure, represented by the slope of isentropes, in cold airmass could also influence the low-level vertical stability. The cold airmass with relatively flat isentropes will likely have a large vertical component of the potential temperature gradient, which is conducive to the reappearance of air pollution.

Further analysis shows that the evolution of the residual cold airmass and the above conditions are mainly associated with the dynamic process rather than diabatic heating/cooling. The strength of the eastward cold airmass flux after CAO is an important factor affecting the decreasing rate of residual cold airmass. This study also investigates the possible indication of large-scale circulation pattern of the CAO during its initial stage in estimating the reappearance of air pollution after CAO. The CAOs driven by the circulation of anticyclonic pattern in northern Siberia (cyclonic pattern in northeastern Asia) usually leads to a rapid (slow) deterioration of air pollution.

Data availability

https://doi.org/10.5194/acp-2022-9
Preprint. Discussion started: 4 April 2022


Atmospheric Chemistry and Physics Discussions

The air quality index (AQI) are available at the Ministry of Ecology and Environment of the People Republic of China (https://air.cnemc.cn:18007/). The JRA-55 reanalysis data is available at Japan Meteorological Agency (https://jra.kishou.go.jp/JRA-55). The sounding data are available at University of Wyoming (http://www.weather.uwyo.edu/upperair/sounding.html).

Acknowledgments

This work was supported by the Guangdong Major Project of Basic and Applied Basic Research (2020B0301030004) and the National Natural Science Foundation of China (NSFC) (Grant 41805122).

References

An, Z., Huang, R. J., Zhang, R., Tie, X., Li, G., Cao, J., Zhou, W., Shi, Z., Han, Y., Gu, Z., and Ji, Y.: Severe haze in northern China: A synergy of anthropogenic emissions and atmospheric processes, Proc. Nat. Acad. Sci. USA, 116, 8657–8666, doi:10.1073/pnas.1900125116, 2019.

An, X., Sheng, L., Liu, Q., Li, C., Gao, Y., and Li, J.: The combined effect of two westerly jet waveguides on heavy haze in the North China Plain in November and December 2015, Atmos. Chem. Phys., 20, 4667–4680, doi:10.5194/acp-20-4667-2020, 2020.

Cao, Z., Sheng, L., Liu, Q., Yao, X., and Wang, W.: Interannual increase of regional haze-fog in North China Plain in summer by intensified easterly winds and orographic forcing, Atmos. Environ., 122, 154–162, doi:10.1016/j.atmosenv.2015.09.042, 2015.

Chen, H., and Wang, H.: Haze days in North China and the associated atmospheric circulations based on daily visibility data from 1960 to 2012, J. Geophys. Res. Atmos., 120, 5895–5909, doi: 10.1002/2015JD023225, 2015.

Dang, R., and Liao, H.: Severe winter haze days in the Beijing–Tianjin–Hebei region from 1985 to 2017 and the roles of anthropogenic emissions and meteorology, Atmos. Chem. Phys., 19, 10801–10816, doi:10.5194/acp-19-10801-2019, 2019.

Ding, A. J., Huang, X., Nie, W., Sun, J. N., Kerminen, V. M., Petäjä, T., Su, H., Cheng, Y. F., Yang, X. Q., Wang, M. H., Chi, X. G., Wang, J. P., Virkkula, A., Guo, W. D., Yuan, J., Wang, Y. S., Zhang, R. J., Wu, Y. F., Song, Y., Zhu, T., Zilitinkevich, S., Kulmala, M., and Fu, C. B.: Enhanced haze pollution by black carbon in megacities in China, Geophys. Res. Lett., 43, 2873–2879, doi:10.1002/2016GL067745, 2016.

Ding, Y., and Liu, Y.: Analysis of long-term variations of fog and haze in China in recent 50 years and their relations with atmospheric humidity, Sci. China Earth Sci., 57, 36–46, doi:10.1007/s11430-013-4792-1, 2014.

Gao, M., Carmichael, G. R., Saide, P. E., Lu, Z., Yu, M., Streets, D. G., and Wang, Z.: Response of winter fine particulate matter concentrations to emission and meteorology changes in North China, Atmos. Chem. Phys., 16, 11837–11851, doi:10.5194/acp-16-11837-2016, 2016.

https://doi.org/10.5194/acp-2022-9
Preprint. Discussion started: 4 April 2022

Guan, W. J., Zheng, X. Y., Chung, K. F., and Zhong, N. S.: Impact of air pollution on the burden of chronic respiratory diseases in China: time for urgent action, Lancet, 388, 1939–1951, doi:10.1016/S0140-6736(16)31597-5, 2016.

Gui, K., Che, H., Wang, Y., Wang, H., Zhang, L., Zhao, H., Zheng, Y., Sun, T., and Zhang, X.: Satellite-derived PM2. 5 concentration trends over Eastern China from 1998 to 2016: Relationships to emissions and meteorological parameters, Environ. Pollut., 247, 1125–1133, doi:10.1016/j.envpol.2019.01.056, 2019.

Guo, J., Zhang, J., Yang, K., Liao, H., Zhang, S., Huang, K., Lv, Y., Shao, J., Yu, T., Tong, B., Li, J., Su, T., Yim, S. H. L., Stoffelen, A., Zhai, P., and Xu, X.: Investigation of near-global daytime boundary layer height using high-resolution radiosondes: First results and comparison with ERA-5, MERRA-2, JRA-55, and NCEP-2 reanalyses, Atmos. Chem. Phys. Discuss. [preprint], doi:10.5194/acp-2021-257, in review, 2021.

Holzworth, G. C.: Mixing depths, wind speeds and air pollution potential for selected locations in the United States, J. Appl. Meteorol., 6, 1039–1044, doi:10.1175/1520-0450(1967)006<1039:MDWSAA>2.0.CO;2, 1967.

Hu, Y., Wang, S., Ning, G., Zhang, Y., Wang, J., and Shang, Z.: A quantitative assessment of the air pollution purification effect of a super strong cold-air outbreak in January 2016 in China, Air Qual. Atmos. Health, 11, 907–923, doi:10.1007/s11869-018-0592-2, 2018.

Iwasaki, T., Shoji, T., Kanno, Y., Sawada, M., Ujiie, M., and Takaya, K.: Isentropic analysis of polar cold airmass streams in the Northern Hemispheric winter, J. Atmos. Sci., 71, 2230–2243, doi:10.1175/JAS-D-13-058.1, 2014.

Kang, H., Zhu, B., Gao, J., He, Y., Wang, H., Su, J., Pan, C., Zhu, T., and Yu, B.: Potential impacts of cold frontal passage on air quality over the Yangtze River Delta, China, Atmos. Chem. Phys., 19, 3673–3685, doi:10.5194/acp-19-3673-2019, 2019.

Li, Q., Zhang, R., and Wang, Y.: Interannual variation of the wintertime fog–haze days across central and eastern China and its relation with East Asian winter monsoon, Int. J. Climatol., 36, 346–354, doi:10.1002/joc.4350, 2016.

Li, Z., Guo, J., Ding, A., Liao, H., Liu, J., Sun, Y., Wang, T., Xue, H., Zhang, H., and Zhu, B.: Aerosol and boundary-layer interactions and impact on air quality, Natl. Sci. Rev., 4, 810–833, doi:10.1093/nsr/nwx117, 2017.

Liu, Q., Cao, Z., and Xu, H.: Clearance capacity of the atmosphere: the reason that the number of haze days reaches a ceiling, Environ. Sci. Pollut. Res., 23, 8044–8052, doi:10.1007/s11356-016-6061-2, 2016.

Liu, Q., Sheng, L., Cao, Z., Diao, Y., Wang, W., and Zhou, Y.: Dual effects of the winter monsoon on haze-fog variations in eastern China, J. Geophys. Res. Atmos., 122, 5857–5869, doi:10.1002/2016JD026296, 2017.

Liu, Q., Chen, G., and Iwasaki, T.: Quantifying the impacts of cold airmass on aerosol concentrations over North China using isentropic analysis, J. Geophys. Res. Atmos., 124, 7308–7326, doi:10.1029/2018JD029367, 2019.

Liu, Q., Liu, Q., and Chen, G.: Isentropic analysis of regional cold events over northern China, Adv. Atmos. Sci., 37, 718–734, doi:10.1007/s00376-020-9226-3, 2020.

Liu, Q., Chen, G., Wang, L., Kanno, Y., and Iwasaki, T.: Southward cold airmass flux associated with the East Asian winter monsoon: diversity and impacts, J. Climate, 34, 3239–3254, doi:10.1175/JCLI-D-20-0319.1, 2021.

https://doi.org/10.5194/acp-2022-9
Preprint. Discussion started: 4 April 2022


Atmospheric Chemistry and Physics Discussions

Ma, S., Shao, M., Zhang, Y., Dai, Q., and Xie, M.: Sensitivity of $PM_{2.5}$ and O_3 pollution episodes to meteorological factors over the North China Plain, Sci. Total Environ., 148474, doi:10.1016/j.scitotenv.2021.148474, 2021.

Petäjä, T., Järvi, L., Kerminen, V. M., Ding, A. J., Sun, J. N., Nie, W., Kujansuu, J., Virkkula, A., Yang, X. Q., Fu, C. B., Zilitinkevich, S., and Kulmala, M.: Enhanced air pollution via aerosol-boundary layer feedback in China, Sci. Rep., 6, 1–6, doi:10.1038/srep18998, 2016.

Qu, W., Wang, J., Zhang, X., Yang, Z., and Gao, S.: Effect of cold wave on winter visibility over eastern China, J. Geophys. Res. Atmos., 120, 2394–2406, doi:10.1002/2014JD021958, 2015.

Shoji, T., Kanno, Y., Iwasaki, T., and Takaya, K.: An isentropic analysis of the temporal evolution of East Asian cold air outbreaks, J. Climate, 27, 9337–9348, doi:10.1175/JCLI-D-14-00307.1, 2014.

Su, T., Li, Z., and Kahn, R.: Relationships between the planetary boundary layer height and surface pollutants derived from lidar observations over China: regional pattern and influencing factors, Atmos. Chem. Phys., 18, 15921–15935, doi:10.5194/acp-18-15921-2018, 2018.

Sun, Y., Chen, C., Zhang, Y., Xu, W., Zhou, L., Cheng, X., ... & Wang, Z.: Rapid formation and evolution of an extreme haze episode in Northern China during winter 2015, Sci. Rep., 6, 1–9, doi:10.1038/srep27151, 2016.

Tang, G., Zhang, J., Zhu, X., Song, T., Münkel, C., Hu, B., Schäfer, K., Liu, Z., Zhang, J., Wang, L., Xin, J., Suppan, P., and Wang, Y.: Mixing layer height and its implications for air pollution over Beijing, China, Atmos. Chem. Phys., 16, 2459–2475, doi:10.5194/acp-16-2459-2016, 2016.

Tie, X., Huang, R. J., Dai, W., Cao, J., Long, X., Su, X., Zhao, S., Wang, Q., and Li, G.: Effect of heavy haze and aerosol pollution on rice and wheat productions in China, Sci. Rep., 6, 1–6, doi:10.1038/srep29612, 2016.

Wang, H. J., and Chen, H. P.: Understanding the recent trend of haze pollution in eastern China: roles of climate change, Atmos. Chem. Phys., 16, 4205–4211, doi:10.5194/acp-16-4205-2016, 2016.

Wang, Y., Yao, L., Wang, L., Liu, Z., Ji, D., Tang, G., Zhang, J., Sun, Y., Hu, B., and Xin, J.: Mechanism for the formation of the January 2013 heavy haze pollution episode over central and eastern China, Sci. China Earth Sci., 57, 14–25, doi:10.1007/s11430-013-4773-4, 2014.

Xu, P., Chen, Y., and Ye, X.: Haze, air pollution, and health in China, Lancet, 382, 2067, doi:10.1016/S0140-6736(13)62693-8, 2013.

Yamaguchi, J., Kanno, Y., Chen, G., and Iwasaki, T.: Cold air mass analysis of the record-breaking cold surge event over East Asia in January 2016, J. Meteor. Soc. Japan, 97, 275–293, doi: 10.2151/jmsj.2019-015, 2019.

Yang, Y., Liao, H., and Lou, S.: Increase in winter haze over eastern China in recent decades: Roles of variations in meteorological parameters and anthropogenic emissions, J. Geophys. Res. Atmos., 121, 13050–13065, doi:10.1002/2016JD025136, 2016.

Yang, Y., Zheng, X., Gao, Z., Wang, H., Wang, T., Li, Y., Lau, G. N. C., and Yim, S. H. L.: Long-term trends of persistent synoptic circulation events in planetary boundary layer and their relationships with haze pollution in winter half year over eastern China, J. Geophys. Res. Atmos., 123, 10991–11007, doi:10.1029/2018JD028982, 2018.

https://doi.org/10.5194/acp-2022-9
Preprint. Discussion started: 4 April 2022


Atmospheric Chemistry and Physics Discussions

Yin, Z., and Wang, H.: Role of atmospheric circulations in haze pollution in December 2016, Atmos. Chem. Phys., 17, 11673–11681, doi:10.5194/acp-17-11673-2017, 2017.

Zhang, X. Y., Wang, Y. Q., Niu, T., Zhang, X. C., Gong, S. L., Zhang, Y. M., and Sun, J. Y.: Atmospheric aerosol compositions in China: spatial/temporal variability, chemical signature, regional haze distribution and comparisons with global aerosols, Atmos. Chem. Phys., 12, 779–799, doi:10.5194/acp-12-779-2012, 2012.

Zhang, X., Sun, J., Wang, Y., Li, W., Zhang, Q., Wang, W., Quan, J., Cao, G., Wang, J., Yang, Y., and Zhang, Y.: Factors contributing to haze and fog in China Chin, Sci. Bull., 58, 1178–1187, doi:10.1360/972013-150, 2013.

Zhang, R., Li, Q., and Zhang, R.: Meteorological conditions for the persistent severe fog and haze event over eastern China in January 2013, Sci. China Earth Sci., 57, 26–35, doi:10.1007/s11430-013-4774-3, 2014.

Zhang, Y., Yin, Z., and Wang, H.: Roles of climate variability on the rapid increases of early winter haze pollution in North China after 2010, Atmos. Chem. Phys., 20, 12211–12221, doi:10.5194/acp-20-12211-2020, 2020.

Zhang, S., Zeng, G., Yang, X., Wu, R., and Yin, Z.: Comparison of the influence of two types of cold surge on haze dispersion in eastern China, Atmos. Chem. Phys., 21, 15185–15197, doi:10.5194/acp-21-15185-2021, 2021.

Zhang, Y., Ma, Z., Gao, Y., and Zhang, M.: Impacts of the meteorological condition versus emissions reduction on the $PM_{2.5}$ concentration over Beijing–Tianjin–Hebei during the COVID-19 lockdown, Atmos. Ocean. Sci. Lett., 14, 100014, doi:10.1016/j.aosl.2020.100014, 2021.

Zhong, W., Yin, Z., and Wang, H.: The relationship between anticyclonic anomalies in northeastern Asia and severe haze in the Beijing–Tianjin–Hebei region, Atmos. Chem. Phys., 19, 5941–5957, doi:10.5194/acp-19-5941-2019, 2019.

https://doi.org/10.5194/acp-2022-9
Preprint. Discussion started: 4 April 2022

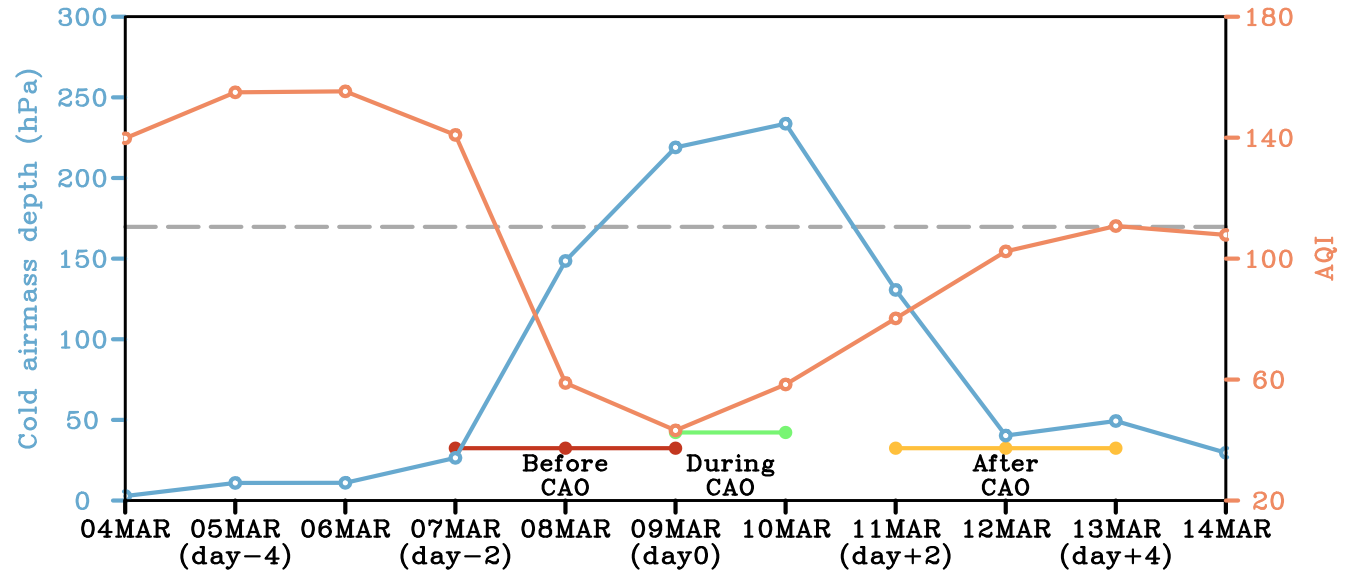

Figure 1: Time series of the regional averaged cold airmass depth (blue line) and AQI (orange line) in North China (114°–122°E, 30°–40°N). The gray dashed line denotes the standard deviation of the cold airmass depth.

https://doi.org/10.5194/acp-2022-9
Preprint. Discussion started: 4 April 2022

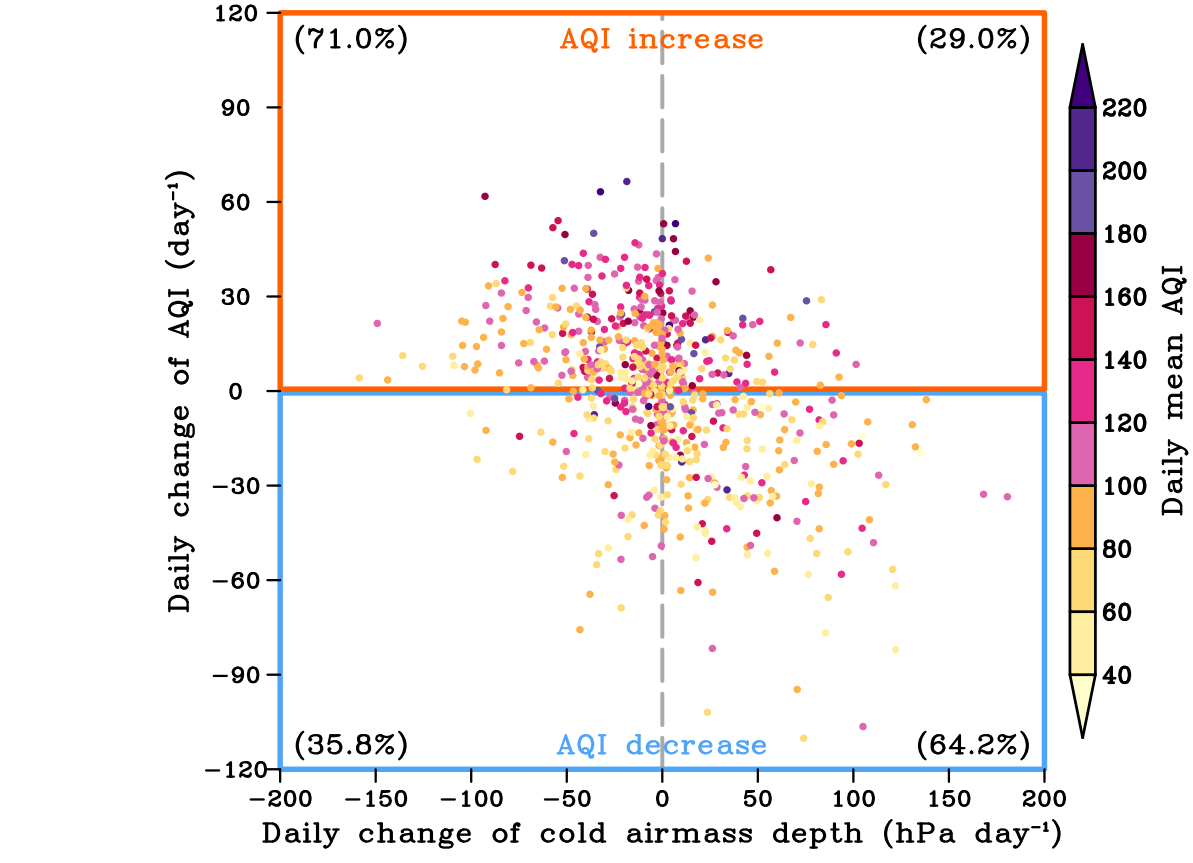

485

Figure 2: Relationship between the daily changes in the AQI and cold airmass depth. The daily change is estimated by the current day minus the preceding day. The colors of the dots denote the daily mean cold airmass depth on the current day.

https://doi.org/10.5194/acp-2022-9
Preprint. Discussion started: 4 April 2022

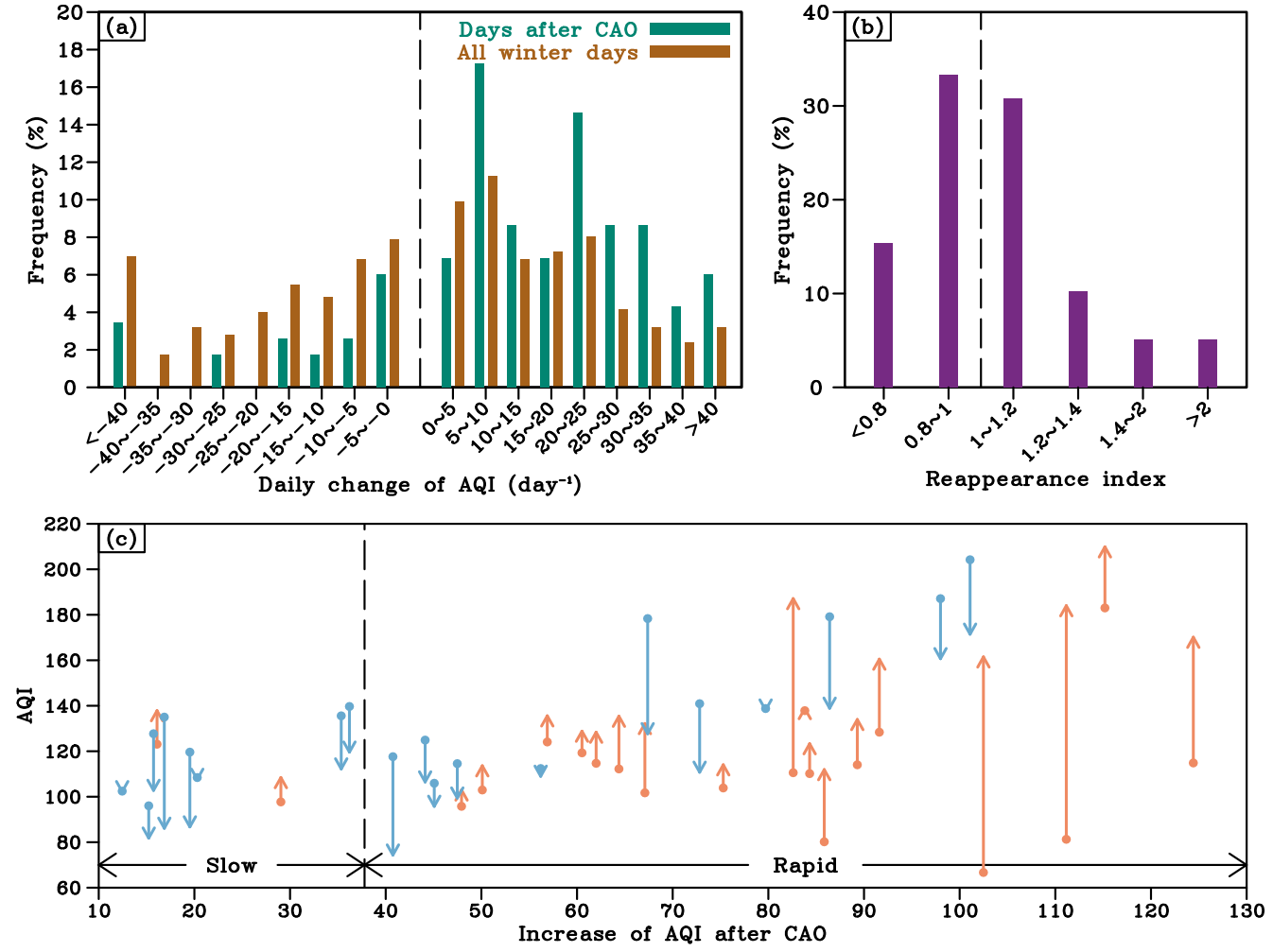

Figure 3: (a) Statistical distribution of daily change of AQI calculated by all of days during the 5 winters (brown bars) and days during the period after the CAOs (green bars). (b) Statistical distribution of the reappearance index of air pollution in 39 CAO events. (c) The increase in the AQI (x-axis) and the change in the AQI from the period before the CAO to the period after CAO (vertical arrows) in 39 CAO events. Black dashed line denotes the standard deviation of AQI. The arrowhead and tail represent AQI_a and AQI_b, respectively. The orange (blue) arrows denote that the AQI worsens (better) after CAO.

https://doi.org/10.5194/acp-2022-9
Preprint. Discussion started: 4 April 2022

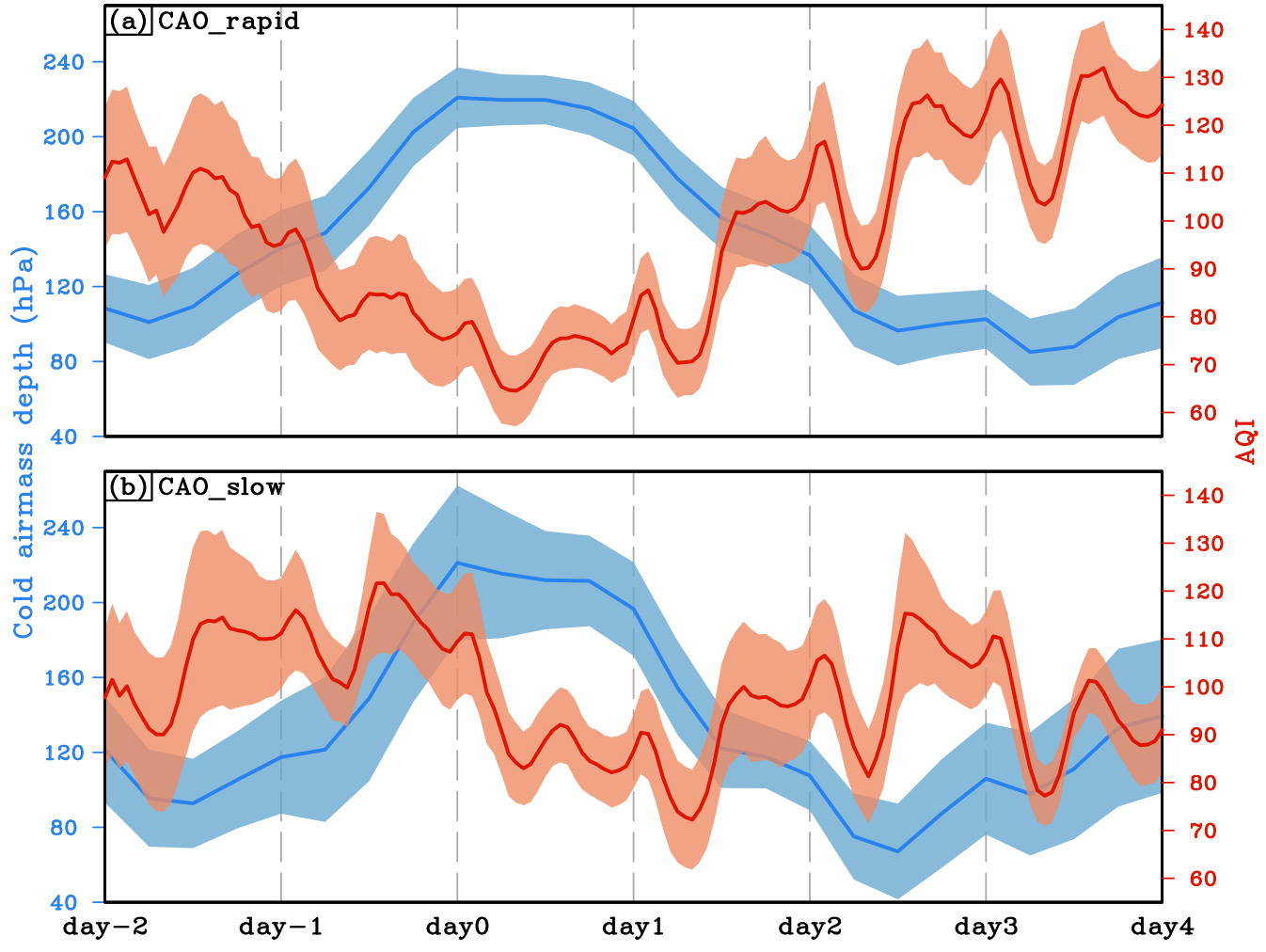

Figure 4: Evolutions of spatially averaged (North China: 114°–122°E, 30°–40°N) cold airmass depth and AQI during CAOs. (a) and (b) are composited by the CAO_rapid events and CAO_slow events, respectively. Shading represents the 95% confidence interval of the composited mean value.

https://doi.org/10.5194/acp-2022-9
Preprint. Discussion started: 4 April 2022

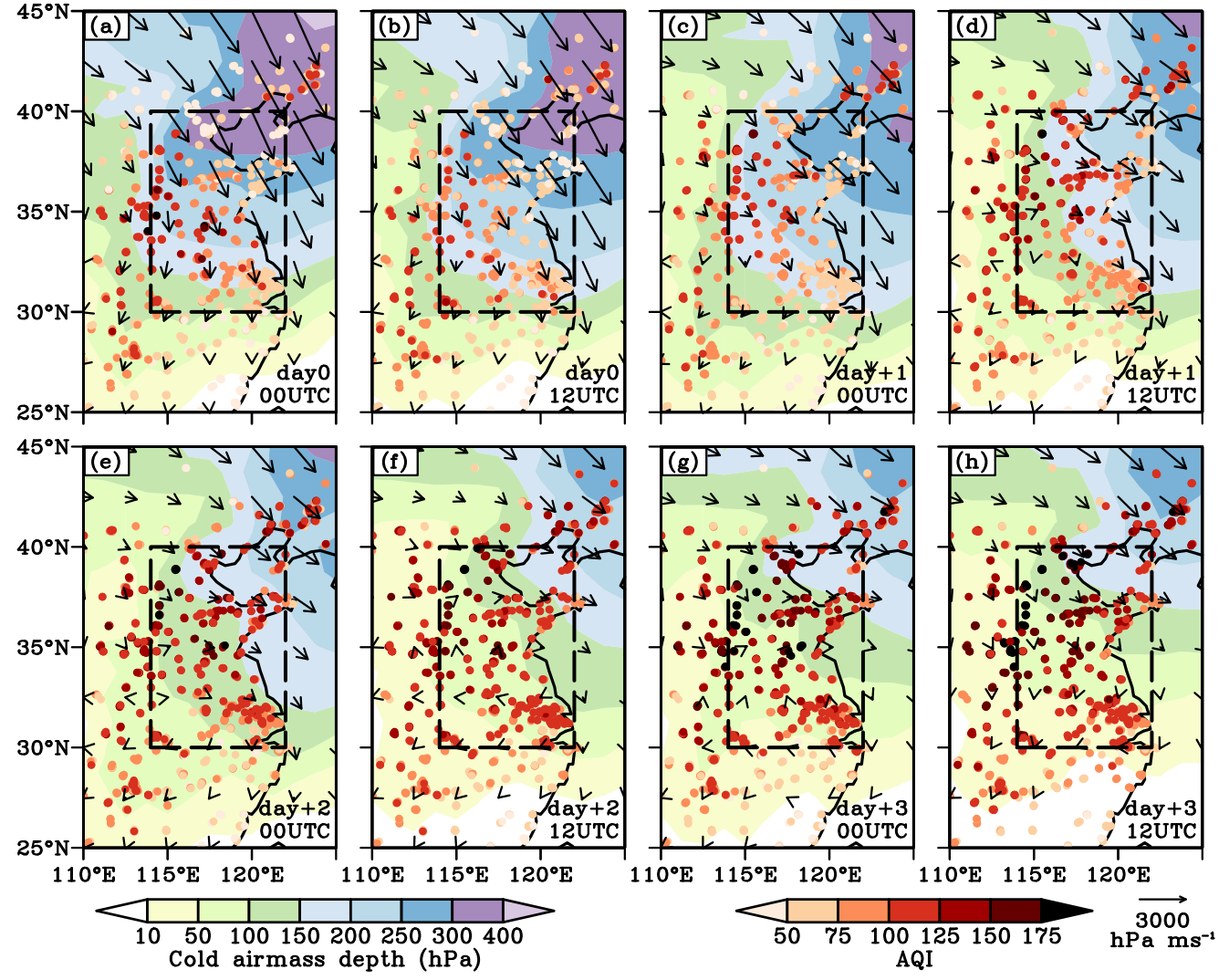

Figure 5: Spatial distributions of the composited cold airmass depth (shaded), horizontal fluxes of the cold airmass (black vectors), and AQI (colored dots) during CAO_rapid events.

https://doi.org/10.5194/acp-2022-9
Preprint. Discussion started: 4 April 2022

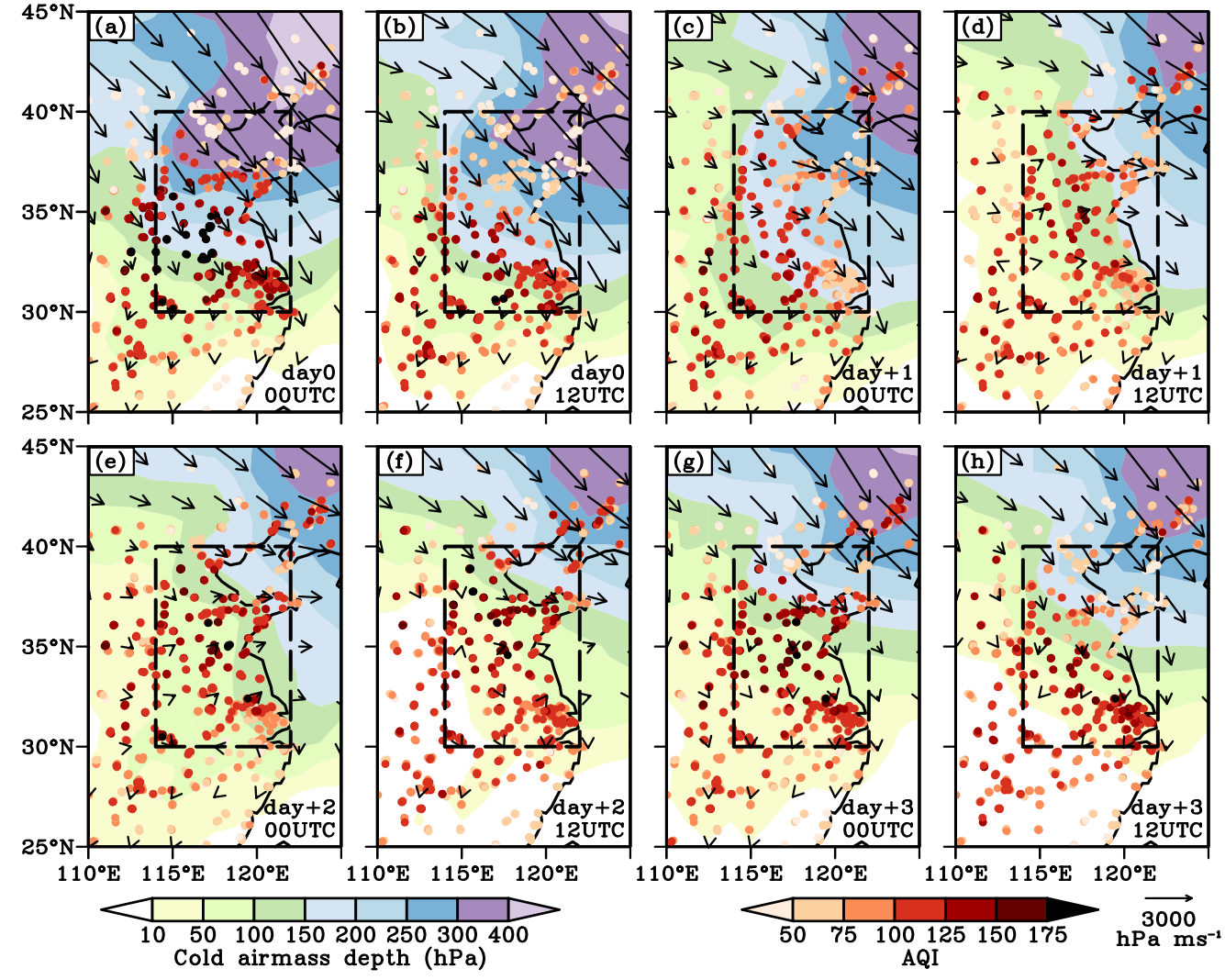

Figure 6: The same as Figure 5 but composited by the CAO_slow events.

https://doi.org/10.5194/acp-2022-9
Preprint. Discussion started: 4 April 2022

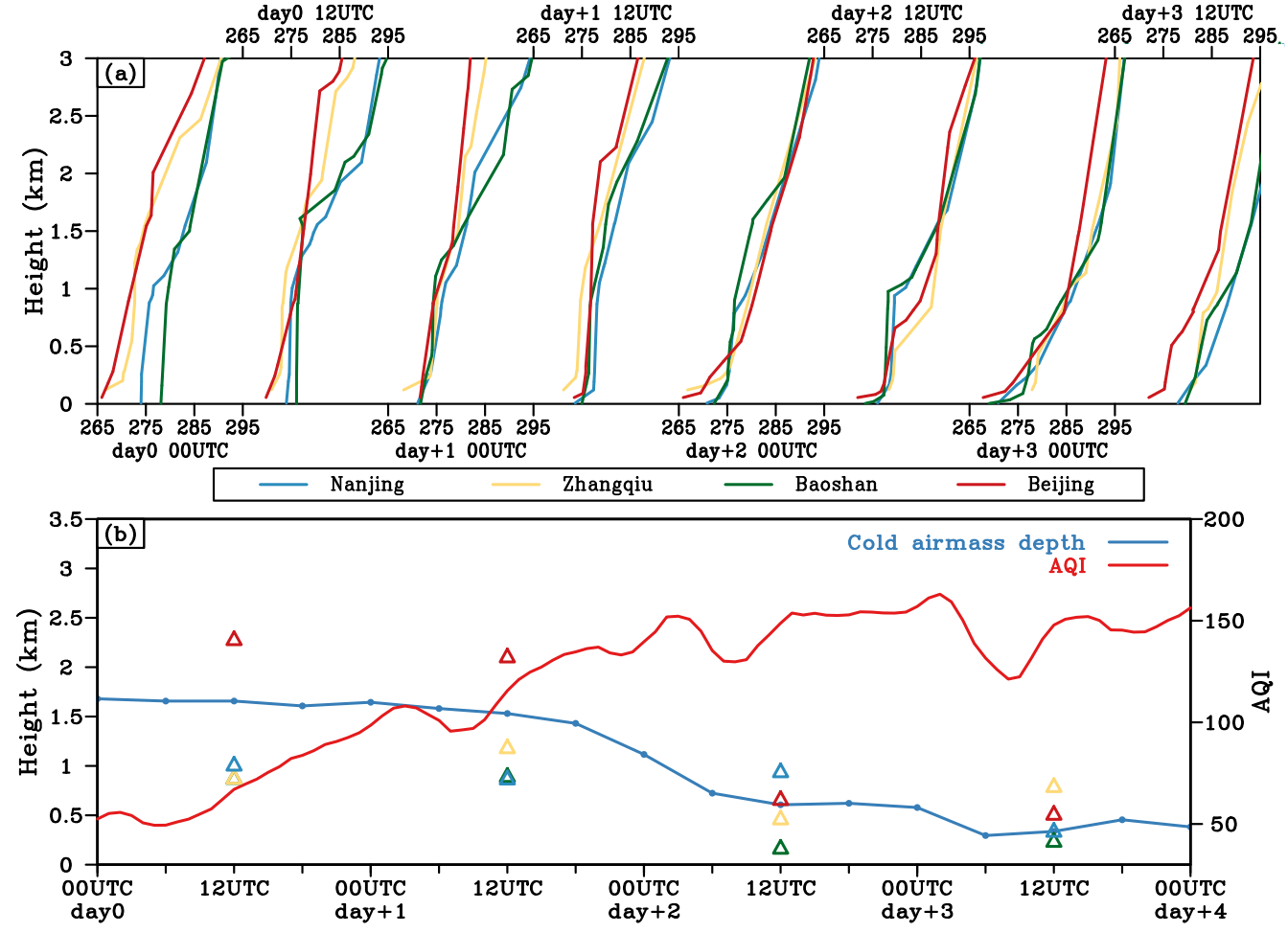

Figure 7: (a) Vertical profiles of potential temperature at four stations (from north to south: Beijing, Zhangqiu, Nanjing, Baoshan) during a CAO rapid event from 14 to 17 Dec 2016. (b) Time series of the regional averaged cold airmass depth and the AQI in North China and MLH (colored triangles) at four stations during a CAO_rapid event from 14 to 17 Dec 2016.

https://doi.org/10.5194/acp-2022-9
Preprint. Discussion started: 4 April 2022

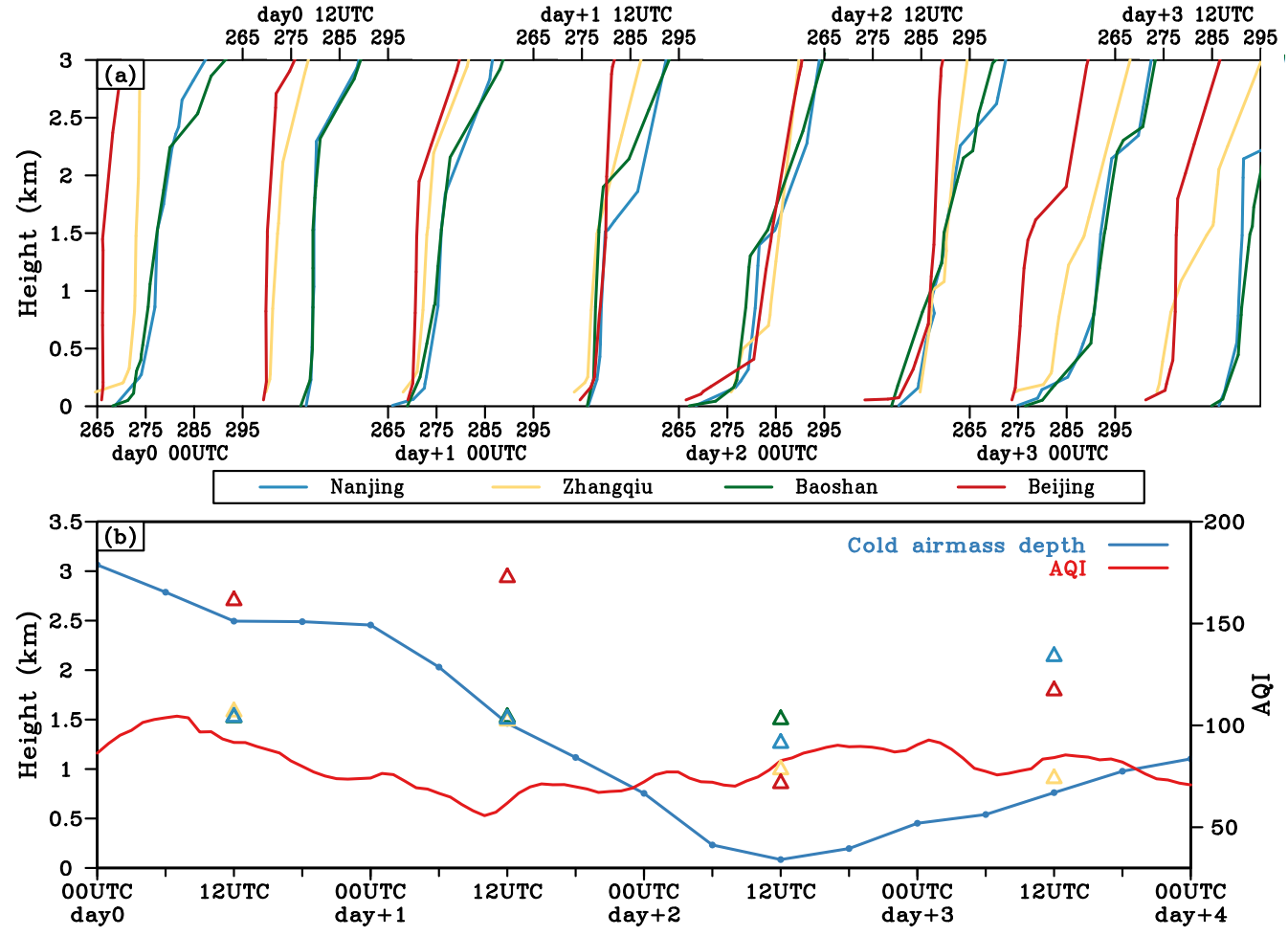

Figure 8: The same as Figure 7 but during a CAO_slow event from 11 to 14 Feb 2018.

https://doi.org/10.5194/acp-2022-9
Preprint. Discussion started: 4 April 2022

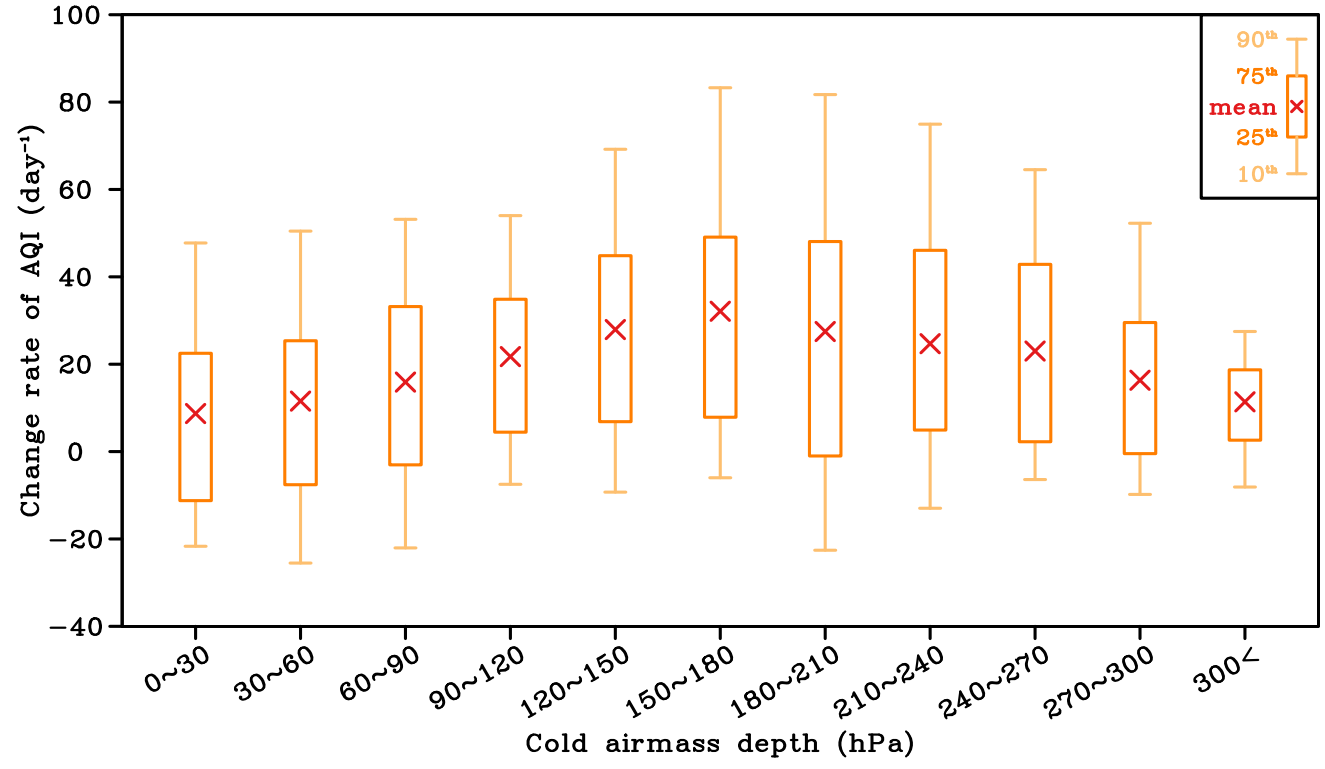

510 **Figure 9: Distribution of the change rate of the AQI with the cold airmass depth during the period after the CAO.**

https://doi.org/10.5194/acp-2022-9
Preprint. Discussion started: 4 April 2022

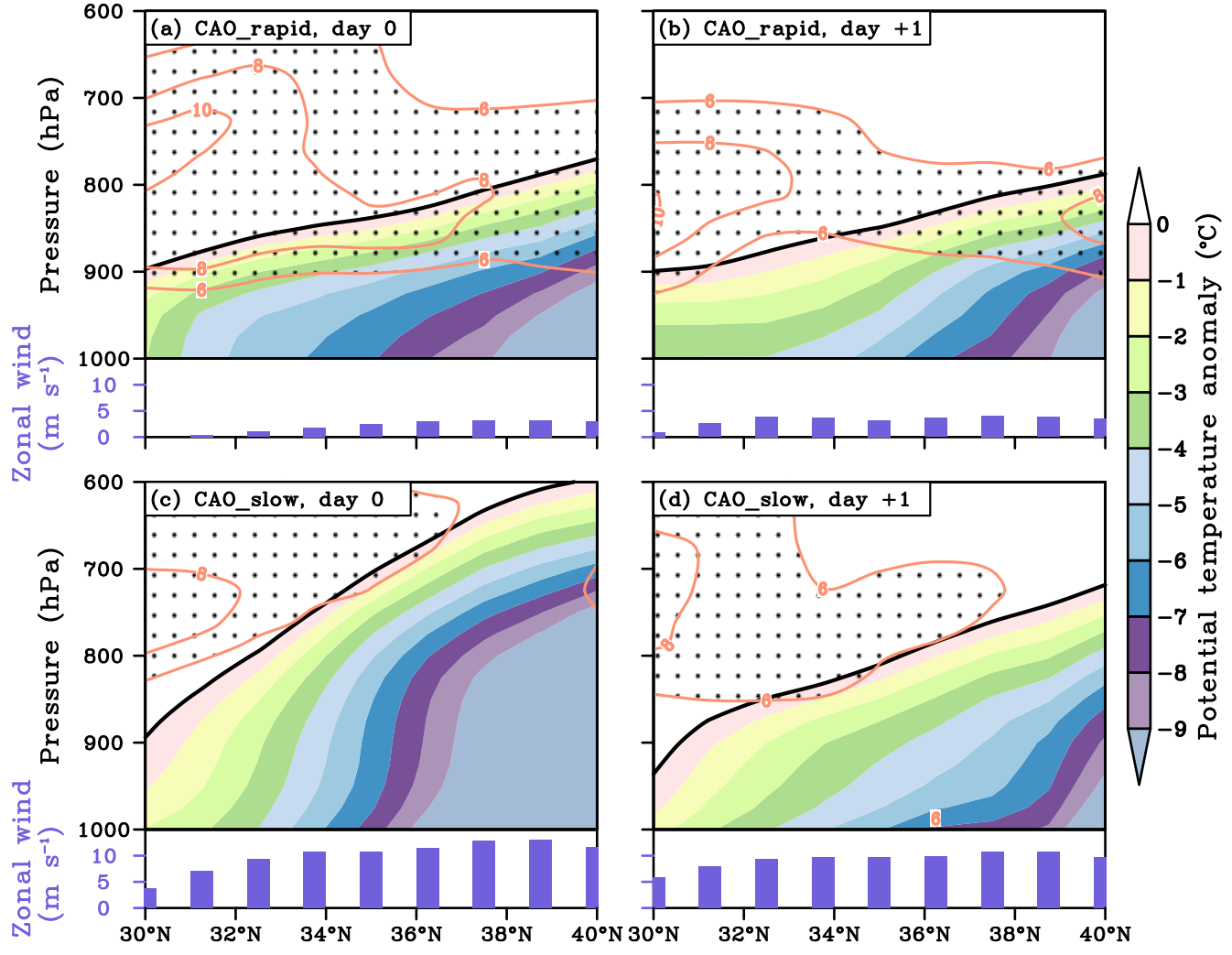

Figure 10: (a, b) Longitude-vertical sections of the potential temperature anomaly (colored shading) and vertical gradient of the potential temperature (contour, unit: $10^{-3}\ K\ m^{-1}$, dotted for $> 6 \times 10^{-3}\ K\ m^{-1}$) along 119°E during the CAO_rapid event from 14 to 17 Dec 2016. The thick black line denotes the upper boundary of cold airmass. The purple bars denote the mean zonal wind speed in the cold airmass. (c, d) The same as (a, b) but during the CAO_slow event from 11 to 14 Feb 2018.

https://doi.org/10.5194/acp-2022-9
Preprint. Discussion started: 4 April 2022

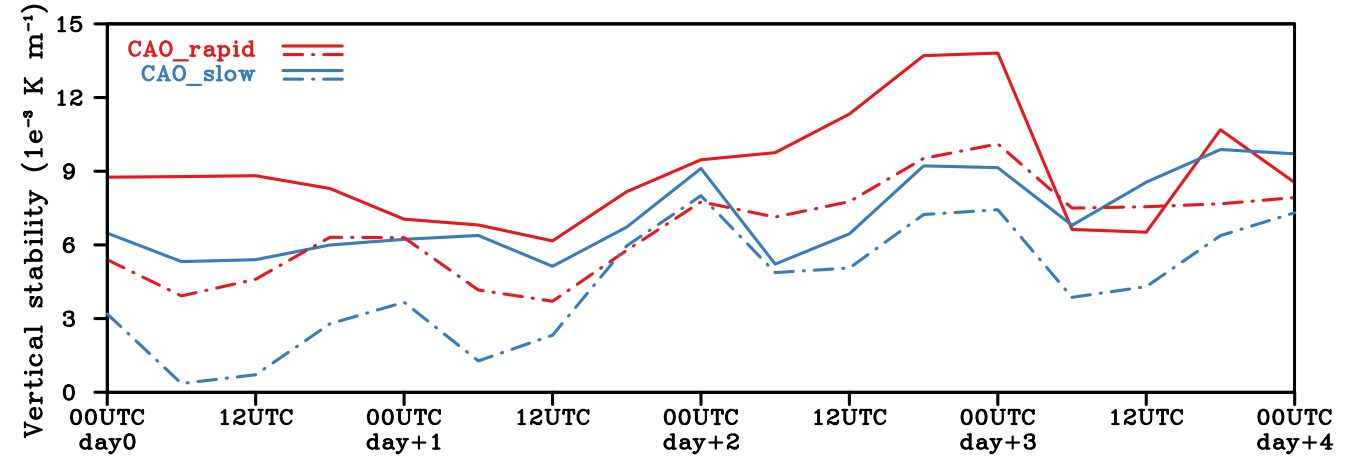

Figure 11: Evolutions of spatially averaged (North China: 114°–122°E, 30°–40°N) vertical stability at the upper boundary of cold airmass (solid line) and the averaged vertical stability in the cold airmass (dash dot line) during a CAO_rapid event from 14 to 17 Dec 2016 (red) and a CAO_slow event from 11 to 14 Feb 2018 (blue).

https://doi.org/10.5194/acp-2022-9
Preprint. Discussion started: 4 April 2022

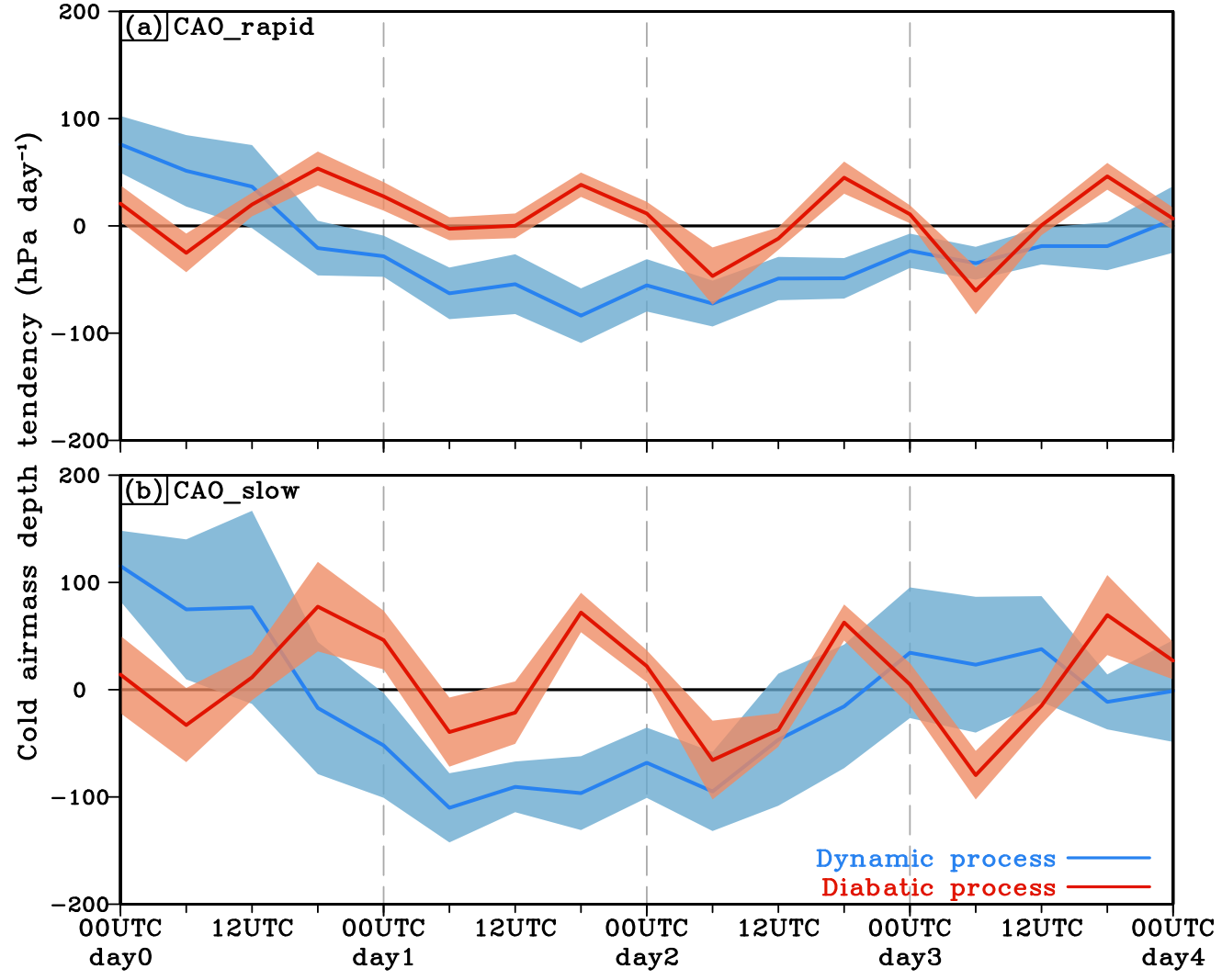

520

Figure 12: Evolutions of the spatially averaged (North China: 114°–122°E, 30°–40°N) cold airmass depth tendency during CAOs. Blue and red lines denote the contributions of dynamic and diabatic processes to the tendency of cold airmass depth, respectively. (a) and (b) are composited by the CAO_rapid events and CAO_slow events, respectively. Shading represents the 95% confidence interval of the composited mean value.

https://doi.org/10.5194/acp-2022-9
Preprint. Discussion started: 4 April 2022

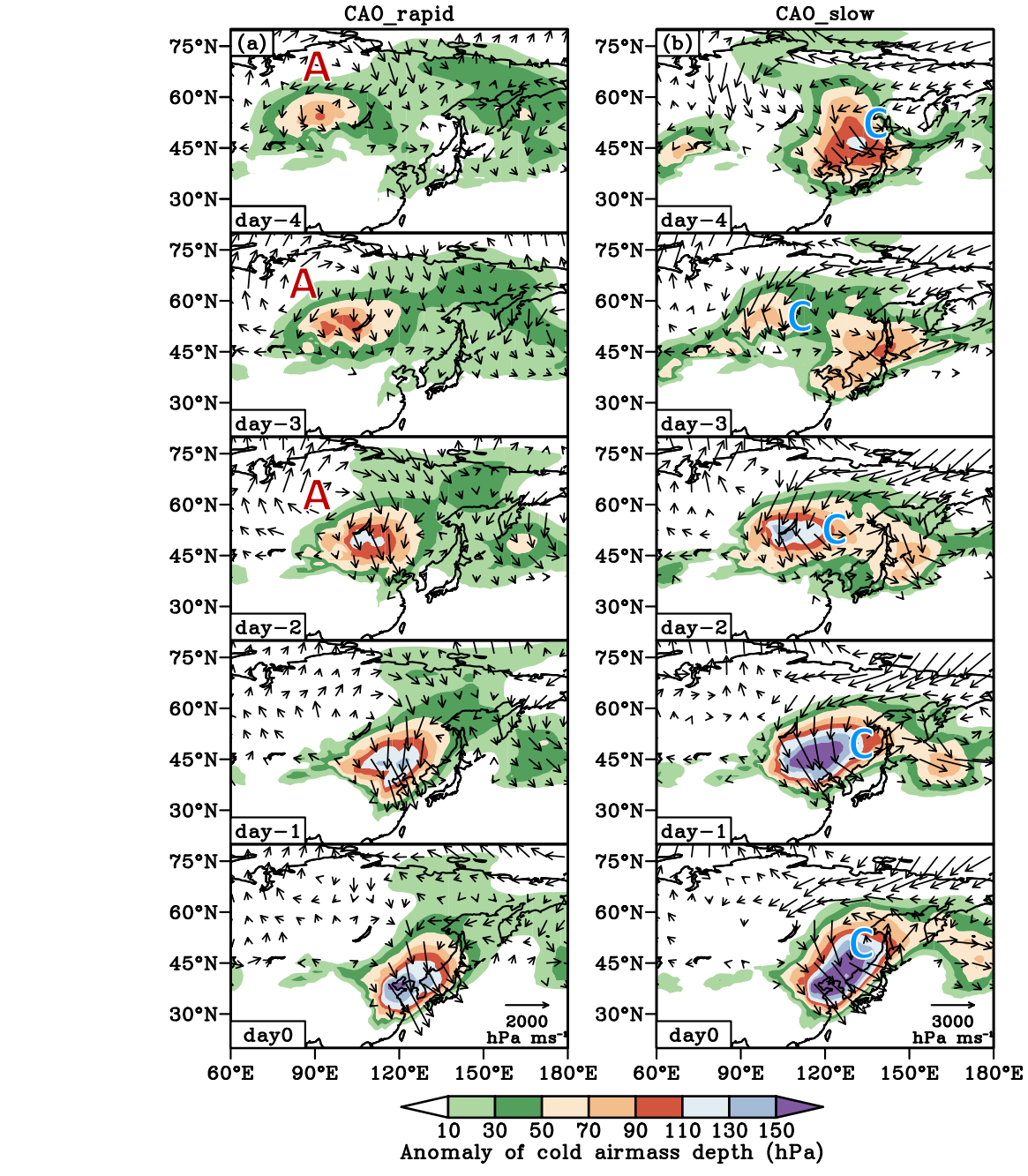

525

Figure 13: Large-scale anomalies of cold airmass depth (shading) and cold airmass flux (vectors) in the initial stage from day −4 to 0. (a) and (b) are composited by the CAO_rapid events and CAO_slow events, respectively.